PROCEEDINGS OF THE ROYAL SOCIETY A
FirstCite® e-publishing

Proc. R. Soc. A
doi:10.1098/rspa.2005.1448
Published online

A topological analysis of the magnetic breakout model for an eruptive solar flare

By Rhona Maclean[1], Colin Beveridge[1], Dana Longcope[2], Daniel Brown[1] and Eric Priest[1]

[1]*Institute of Mathematics, University of St Andrews, The North Haugh, St Andrews, Fife, KY16 9SS, UK*
(rhonam@mcs.st-and.ac.uk)
[2]*Department of Physics, Montana State University, Bozeman, MT 59717-3840, USA*

The magnetic breakout model gives an elegant explanation for the onset of an eruptive solar flare, involving magnetic reconnection at a coronal null point which leads to the initially enclosed flux 'breaking out' to large distances. In this paper we take a topological approach to the study of the conditions required for this breakout phenomenon to occur. The evolution of a simple delta sunspot model, up to the point of breakout, is analysed through several sequences of potential and linear force-free quasi-static equilibria. We show that any new class of field lines, such as those connecting to large distances, must be created through a global topological bifurcation and derive rules to predict the topological reconfiguration due to various types of bifurcation.

Keywords: solar flare; magnetic breakout; magnetic topology; solar corona

1. Introduction

Explaining the origin and evolution of solar flares is essential if we wish to gain a complete understanding of the dynamic nature of the solar atmosphere. Many contending theories have been put forward to account for solar flare initiation, including loss of equilibrium (Klimchuk & Sturrock 1989; Priest & Forbes 1990), tether cutting (Moore *et al.* 2001), the effect of the kink instability (Gerrard & Hood 2003; Török *et al.* 2004) and the magnetic breakout model. Each of these theories has been developed over the course of several years and has undergone intense scrutiny in the attempt to find the most accurate model for the onset of a solar flare. It is fair to say that the debate is still open.

Here, we choose to study and develop further the magnetic breakout model, as first proposed by Antiochos *et al.* (1999). In this model, a central flux system is initially enclosed by an overlying arcade. Shear is applied near a neutral line in the photosphere, causing magnetic reconnection to take place in the vicinity of a magnetic null point in the corona. This weakens the overlying field and allows the originally enclosed flux to 'break out' explosively.

Further work by Antiochos (1998) showed that the simplest configuration with sufficient complexity to allow this behaviour is the delta sunspot. A delta sunspot consists of two opposite-polarity sunspot umbrae contained within a common

Received 4 June 2004
Accepted 13 December 2004

penumbra. Indeed, such a configuration is observed to be a prolific producer of flares. For example, Tanaka (1991) showed that significant flares were produced by 90% of delta groups with inverted polarity (e.g. Zhang 1995).

In this paper, we will model a delta sunspot using the principles of *magnetic charge topology* (MCT) (Longcope 1996). MCT is based on three principal simplifying assumptions (which were justified in Longcope's paper):

(i) magnetic flux concentrations in the photosphere are represented as point sources;
(ii) these sources are assumed to lie in the plane $z=0$, representing the photosphere, with the corona considered to be the half-space $z>0$;
(iii) the magnetic field is approximated by a potential or linear force-free field.

What is the value of such an MCT model by comparison with the full dynamic MHD breakout model of Antiochos *et al.* (1999)? There are several issues here. The idea is that a slow evolution of pre-eruptive magnetic configuration (through a series of equilibria in response to, for instance, photospheric footpoint motions or flux emergence) leads to a dynamic eruptive phase in which the magnetic field breaks out. Although the slow pre-eruptive evolution can be described accurately by studying a series of equilibria, the dynamic phase itself needs the full resistive MHD equations. Work done by Zhang & Low (2001, 2003) has given us a more complete physical picture of the full eruption, through the initial, dynamical and final relaxed states. However, the breakout model is largely numerical, and it is important to try to develop a deeper understanding of the conditions for the initiation of the eruptive phase. What are the conditions for onset? What are the topological features of the pre-eruptive and post-eruptive configurations? It is our purpose to try to shed a little light on these questions by using the MCT model, while recognizing that it will not reproduce many of the detailed features of a fully dynamic model.

Using discrete sources is a key assumption in our analysis. It is a reasonable model when the major sources of flux are sunspots, and also in the quiet Sun, where most of the photospheric flux is in the form of discrete isolated intense sources. It is only when the sources are discrete that the notion of different topologies—i.e. regions where there are different sources of flux separated by separatrix surfaces that intersect in separators—comes into its own. If the photospheric flux were continuously distributed everywhere, then there would be only one source, namely, the whole (positively signed, say) photosphere. Nevertheless, it was recognized by Priest & Démoulin (1995) and later developed by Démoulin *et al.* (1996) and Titov *et al.* (2002) that, even when the sources are continuous, there can sometimes be remnants of separatrices and separators (called quasi-separatrix layers and quasi-separators) at which the mapping gradient is large rather than discontinuous, and which behave in very similar ways to their discrete counterparts.

Although the magnetic field in much of the corona is likely to be close to potential, this is not true at low altitudes or in sheared structures such as prominences or the delta sunspots studied here. Owing to flux emergence or movement of footpoint locations, the coronal field can gain a net twist which probably remains trapped there as a result of the high magnetic Reynolds

number in the corona. This is not dealt with by the potential field model. However, it is often true (Longcope & Magara 2004) that the positions of topological features, as calculated using MCT, closely approximate the positions found by a full MHD simulation. At the very least, the features present in an MCT model provide an invaluable guide for understanding results gained from more complex nonlinear force-free or full MHD simulations. Also, it is much easier to explore a wider range of parameter space with the MCT model. Having said this, clearly the energy released in flares must come from a non-potential field if the photospheric normal magnetic field component remains constant during a flare. Typically, the difference between estimates of active region energies and those of a potential field with the same photospheric magnetic field are small; of the order of 15% (e.g. Gary *et al.* (1987) found a difference of around 10%, while Klimchuk & Sturrock (1992) found a difference of 20%).

MCT models the field's topology, defined as the property which is invariant under continuous deformation. Thus, the topology of a potential field will be identical to the topologies of all non-potential fields with sufficiently small current densities. When the current density becomes large enough to change the topology, this change must occur as a bifurcation. However, the same bifurcation can occur in a continuous sequence of potential fields, although the exact parameter values at which changes between topological states occur will naturally vary, depending on the form of $\alpha(\boldsymbol{r})$ (Brown & Priest 2000). The present work concerns the particular bifurcation leading to magnetic breakout when the field is sheared. For simplicity, we choose first to characterize this bifurcation in a sequence of potential fields and later will demonstrate the identical bifurcation in non-potential fields.

In view of this, we choose to consider initially a magnetic field such that $\boldsymbol{B}=-\boldsymbol{\nabla}\Phi$, where Φ is a scalar potential. We can then write the field explicitly at any point in the corona owing to n point sources in the solar surface with magnetic field strengths ε_i at positions $\boldsymbol{r}_i (i=1, \ldots, n)$. At position $\boldsymbol{r}$ it is given by

$$\boldsymbol{B}(\boldsymbol{r}) = \sum_{i=1}^{n} \varepsilon_i \frac{\boldsymbol{r}-\boldsymbol{r}_i}{|\boldsymbol{r}-\boldsymbol{r}_i|^3}. \tag{1.1}$$

Points where the magnetic field vanishes are called *null points*, and have been studied in detail by Parnell *et al.* (1996). A system of coordinates can be found such that the first-order linear field near any null point can be written as $\boldsymbol{B}=\boldsymbol{M}\cdot\boldsymbol{r}$, where $\boldsymbol{r}=(x, y, z)^{\mathrm{T}}$ and

$$\boldsymbol{M} = \begin{pmatrix} \dfrac{\partial B_x}{\partial x} & \dfrac{\partial B_x}{\partial y} & \dfrac{\partial B_x}{\partial z} \\ \dfrac{\partial B_y}{\partial x} & \dfrac{\partial B_y}{\partial y} & \dfrac{\partial B_y}{\partial z} \\ \dfrac{\partial B_z}{\partial x} & \dfrac{\partial B_z}{\partial y} & \dfrac{\partial B_z}{\partial z} \end{pmatrix} = \begin{pmatrix} 1 & \dfrac{1}{2}(q-j_{\parallel}) & 0 \\ \dfrac{1}{2}(q-j_{\parallel}) & p & 0 \\ 0 & j_{\perp} & -(p+1) \end{pmatrix}. \tag{1.2}$$

Here, $j_{\parallel}$ and $j_{\perp}$ are the currents parallel and perpendicular to the spine of the null point (defined below), while p and q are parameters of the potential field. In the potential case we consider, $j_{\parallel}$ and $j_{\perp}$ vanish.

In view of the solenoidal condition ($\nabla \cdot \boldsymbol{B}=0$), the trace of $\boldsymbol{M}$ (and hence the sum of the eigenvalues) must vanish. In the potential case, all three eigenvalues are real; ignoring the degenerate cases where one or three eigenvalues vanish, it is clear that one eigenvalue (λ_1) must be of opposite sign to the other two (λ_2 and λ_3). The eigenvector ($\hat{\boldsymbol{e}}_1$) associated with λ_1 defines an isolated field line called the *spine*; the other two eigenvectors ($\hat{\boldsymbol{e}}_2$ and $\hat{\boldsymbol{e}}_3$) define the *fan plane* of the null point (Priest & Titov 1996); field lines beginning in the fan plane form the *separatrix surface*.

These, along with the separators (defined below), constitute the *skeleton* of the null point (Priest *et al.* 1997). The skeleton of a magnetic configuration consists of the extensions of the skeletons of all of its null points.

The null is classified as *positive* if λ_2 and λ_3 are positive, and *negative* otherwise. The spines of a positive null point begin at positive sources and end at the null; those beginning at a negative null point end at negative sources. In either case, these sources are the null's spine sources; if they are distinct, the null is *heterospinal*, whereas if both spines end at the same source, the null is *homospinal* (Beveridge 2003). In addition, if the spine of a null point lies in the photospheric plane, it is labelled *prone*, as opposed to *upright* if the spine is perpendicular to it or *coronal* if it lies outside the photosphere (Longcope & Klapper 2002).

The separatrix surface of a heterospinal null divides space into different regions of connectivity, or *flux domains*. Field lines on either side of the surface will begin (or end) at the spine sources of the null.

A *separator* is a field line connecting a positive and a negative null point. It is the three-dimensional analogue of a two-dimensional X-point and is a prime location for reconnection (Greene 1988; Lau & Finn 1990; Priest & Titov 1996; Galsgaard & Nordlund 1997). Separators generally lie along the boundaries between four different regions of connectivity—at least for separators connecting heterospinal nulls. Such a separator is called a *proper separator*. It can be shown that a separator only links two null points if the separatrix of one contains both spines of the other (Beveridge *et al.* 2005). If a null point has no separators, its fan plane is referred to as *unbroken*; otherwise it is known as *broken* (Longcope & Klapper 2002).

The numbers of various elements of a field's skeleton are linked by several relationships. In a situation with flux balance, the field at a great distance from the sources is approximately dipolar. On a contour of sufficiently large diameter, the Kronecker–Poincaré index (χ) of the field will be two (Molodenskii & Syrovatskii 1977). Then, the Euler characteristic equation,

$$M - c + m = \chi, \tag{1.3}$$

holds in the photospheric plane. Here, M is the number of potential maxima (e.g. Inverarity & Priest 1999), m is the number of minima, and c is the number of saddle points. Saddle points of the potential correspond to prone nulls, maxima correspond to either positive sources or positive upright nulls, and minima correspond to either negative sources or negative upright nulls. This allows us to relate the numbers of sources (S), prone

nulls (n_{p}) and upright nulls (n_{u}) by the two-dimensional Euler characteristic

$$S + n_{\mathrm{u}} = n_{\mathrm{p}} + 2, \tag{1.4}$$

which holds when the net flux in the source plane is zero. The properties of nulls in three-dimensional space are governed by the three-dimensional Euler characteristic

$$S_+ - n_+ = S_- - n_-, \tag{1.5}$$

where $S_\pm$ represents the number of positive or negative sources and $n_\pm$ the number of positive or negative nulls. In both of these equations, flux balance is assumed; for an unbalanced case, it is necessary to add a balancing source at a great distance and increase S, as well as S_+ or S_-, appropriately.

Longcope & Klapper (2002) found a relationship between the number of flux domains (D), separators (X), null points (n) and sources (S),

$$D = X - n + S, \tag{1.6}$$

where n excludes homospinal nulls and nulls with unbroken fans. However, this result applies to the whole of space rather than to the coronal half-space. For a result in the latter, we must differentiate between *photospheric domains*, which contain field lines which lie in the photosphere, and *purely coronal domains*, which do not. Making this distinction, we can modify the equation to

$$D_\phi + 2D_{\mathrm{c}} = 2X - n_\phi - 2n_{\mathrm{c}} + S, \tag{1.7}$$

where D_ϕ is the number of photospheric domains, D_{c} the number of purely coronal domains, n_ϕ the number of photospheric nulls and n_{c} the number of coronal nulls (Beveridge 2003). Again, homospinal nulls and nulls with unbroken fans are excluded.

By changing the source strengths and positions of the sources, it is possible to force a change from one topological state to another—for instance, by creating a pair of null points or by allowing two separatrix surfaces to intersect, giving rise to a separator. Several different types of bifurcation are possible, in the following two distinct classes.

(i) Local bifurcations in which the number of nulls changes. Local bifurcations can, and usually do, have global effects.
(ii) Global bifurcations in which the structure of the field changes, but the number of nulls does not.

The final tools of MCT which we will require are the *domain* and *null graphs*, introduced by Longcope (2001) and Longcope & Klapper (2002), respectively. The domain graph has as vertices all of the flux sources; a pair of vertices is connected if and only if field lines connect the two flux sources they represent. The null graph has as its vertices all of the null points; two vertices are connected if and only if the null points they represent are connected by a separator. With these tools at our disposal, it is possible to catalogue quite complex topologies with some confidence.

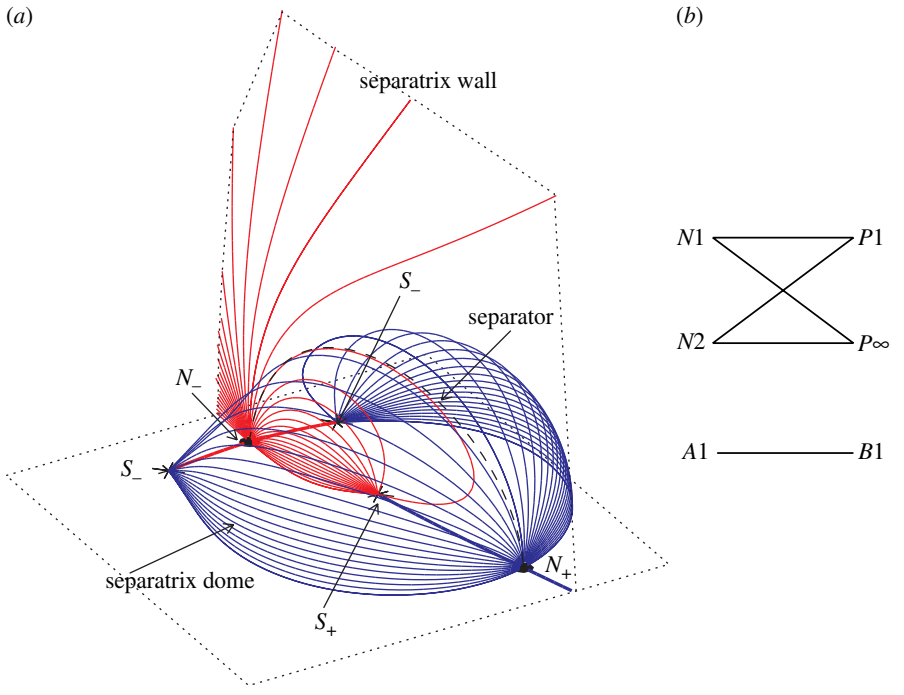

Figure 1. (*a*) Three-dimensional view of the intersecting topology: spines are thick lines, separatrix field lines are thin lines and the separator is a dashed line. (*b*) Domain graph (above) and null graph (below) for the intersecting topology. *P* stands for positive source, *N* for negative source, *B* for positive null and *A* for negative null. (This is the standard notation.) In the domain graph, two sources are linked if they share flux; in the null graph, two nulls are linked if they are joined by a separator.

As an illustrative example, the skeleton of a typical three-source intersecting state (Brown & Priest 1999) is shown in figure 1*a*. Its domain and null graphs are also given in figure 1*b*. The topology consists of one positive and two negative sources, plus the balancing source required at infinity. The two negative sources are fairly close together; their combined strength is greater than the strength of the positive source, so a separatrix dome is formed. A separatrix wall also exists, between the two negative sources and stretching off to infinity in either direction, which intersects the dome (hence the name of the state). Two null points are formed: a negative one between the two negative sources and a positive one at the opposite end of the dome. A separator links the nulls; it is the intersection between the separatrix surfaces.

In the following section, we will outline our simple model for a delta sunspot and detail the numerical, which §3 will show to be responsible for most of the topological breakout behaviour observed. We will conclude with a discussion of our results.

2. Models and bifurcation analysis

We model a delta sunspot with an unbalanced six-source configuration. Table 1 and figure 2 show the initial arrangement of sources used. The positions

Table 1. *Initial source positions and strengths for our model*

source	position	strength
$P1$	(0, 0)	ε
$N1$	(0, 1)	-1
$N2$	(0.866, -0.5)	-1
$N3$	(-0.866, -0.5)	-1
$P2$	(0, -3)	2.5
$P3$	(2.5, 1.5)	2.5

and strengths given are all relative numbers. A central, positive source is surrounded by three negative sources, which are in turn flanked by two strong positive sources. This simulates the emergence of a new area of positive flux into a pre-existing simple sunspot configuration to form a delta spot.

In this initial state, all the flux from $P1$ goes to $N1$, $N2$ and $N3$; none of it connects out to $N\infty$, the balancing source at infinity. It is prevented from doing so by the presence of two separatrix domes which entirely enclose the flux in the central region. The outer dome is formed by the separatrix surface of the null $A1$, which touches the photosphere along the circuit $A1$–$P3$–$B1$–$P2$–$A1$. The inner dome consists of the separatrix surfaces of the coronal nulls $B2$ and $B3$; they touch along the spine $N1$–$A5$–$N2$ and the whole dome is bounded in the photosphere by the circuit $A2$–$N1$–$A4$–$N2$–$A3$–$N3$–$A2$.

The topological manifestation of a breakout is the addition of a flux domain which connects the central, originally enclosed, source to the balancing source at infinity. We shall attempt to provoke such behaviour by disturbing the configuration in three ways:

(i) by altering the strength of the central source in a potential field, from just above 0 up to 2;
(ii) by altering the location of the central source in a potential field, within a 2×2 square centred on the origin;
(iii) by altering the parameter α of a force-free field, while keeping $P1$ fixed near the origin with $\varepsilon=1.5$.

Each progression is marked by a sequence of *bifurcations* at which the field's topology changes. Each bifurcation can be classified as either local or global, as described in §1. In a local bifurcation the number of nulls changes, but the connectivity of the field remains unchanged, i.e. the domain graph is unaffected. This is an essential, and indeed defining, property of a local bifurcation. Of course, the creation of new null points means new separatrix surfaces also appear in the topology but these cannot be created in such a way as to change the existing domain structure. However, local bifurcations do change the number of proper separators, X, according to

$$\Delta X = \Delta n_{\mathrm{c}} + \frac{1}{2}\Delta n_{\phi} \quad \text{(local bifurcation)}. \tag{2.1}$$

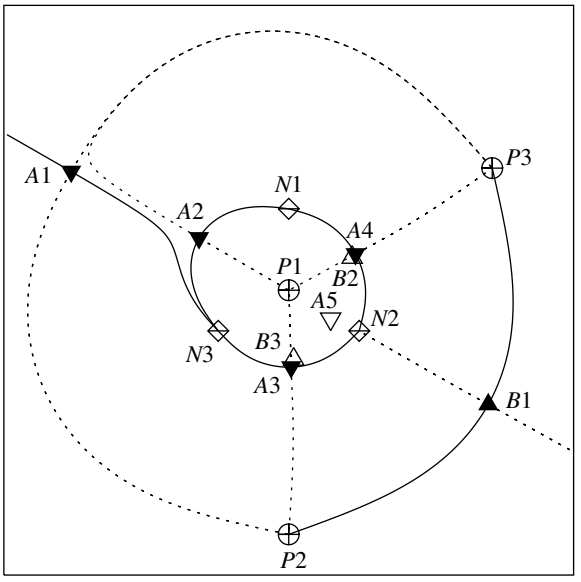

Figure 2. The initial state for our model, with the strength ε of the central source set equal to 1.5. The view here is the so-called 'footprint' of the topology, namely, a plan view of the field lines in the photosphere. Positive sources are circles (labelled P) and negative sources are diamonds (labelled N). Photospheric nulls are solid triangles, while coronal nulls are open triangles. The triangles for positive nulls (labelled B) point upwards, while those for negative nulls (labelled A) point downwards. Spines are indicated by continuous lines and intersections of the separatrix surface with the photosphere are dotted lines.

This is the difference of equation (1.7) after noting that $\Delta S = \Delta D = 0$. It is a general rule which tells us about the effect a local bifurcation will have on a given topology, and can be applied to predict the change in the number of separators we expect to find, given information about the number of null points created or destroyed. The change in the number of photospheric nulls, $\Delta n_\phi = \Delta n_+ + \Delta n_-$, will always be an even number since the difference of equation (1.5) yields $\Delta n_+ = \Delta n_-$. (Upright nulls are always *homospinal nulls* and are therefore not counted among photospheric nulls in equation (1.7).)

Although it is not yet possible to observe directly the topological structure of the corona, various techniques to reconstruct it from photospheric magnetic field data exist. Rules such as this one for local bifurcations provide a useful check on the accuracy of these reconstructions. Indeed, in the future it may become possible to observe separatrices and separators in the corona owing to the large current accumulation expected there (McLaughlin & Hood 2004), in which case such rules would come into their own.

The term breakout refers to the creation of a new domain connecting to distant sources. This must occur as a *global* bifurcation, since local bifurcations do not change the domain structure. In all three cases we consider, this new domain can be created through a global spine-fan bifurcation (Brown & Priest 1999). In a global spine-fan bifurcation, the spine of one null sweeps across the fan of a second like-signed null. In the examples shown in figure 3 the spine

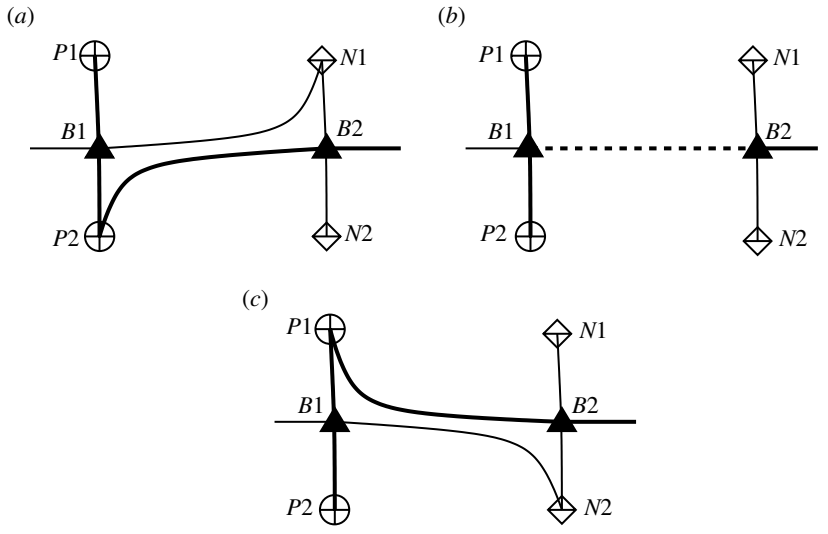

Figure 3. An example of the global spine-fan bifurcation shown as a footprint in the $z=0$ plane, with positive sources $P1$ and $P2$, negative sources $N1$ and $N2$, and positive nulls $B1$ and $B2$. Thick lines are spines, thin lines are the intersection of the separatrix surfaces with the $z=0$ plane and the dotted line is a separator. This bifurcation is designated $B2 \dashv B1$.

connecting null $B2$ to source $P2$ approaches null $B1$ (figure 3*a*). At the instant of bifurcation (figure 3*b*) the spine actually joins the fan, thereby connecting $B2$ to $B1$ in a structurally unstable topology (Hornig & Schindler 1996). Immediately following this, the spine of $B2$ connects to $P1$ as shown in figure 3*c*.

A general global spine-fan bifurcation 'flips' the spine γ of one null, S, between two sources. These sources are the two *spine sources* of the second null T, across whose fan γ has flipped. The global consequences of this bifurcation, which we designate $S \dashv T$, result from changing separators as follows. Each separator connected to S will also connect to an opposing null S'. One *sector* Σ of the S' fan will be bounded by this separator and the spine γ (Longcope & Klapper 2002). The fan sector Σ remains bounded by γ, even as it flips through the T fan; the spine 'drags' the fan sector with it. Consider first a case where Σ did not intersect the T fan before the bifurcation. The spine γ will then 'drag' the fan sector Σ through the T fan as it flips, thereby introducing a new separator linking T to S' (the separator is the new intersection). Had such an intersection been present previously, the bifurcation would eliminate it (running the creation scenario in reverse), thereby destroying the T–S' separator. In this manner the global spine-fan bifurcation $S \dashv T$ creates and destroys separators, changing their total number by ΔX. Since neither the sources nor the nulls are affected,[1] the number of domains

[1] There is an exception to this rule in cases where null T has an *unbroken fan* either before or after the bifurcation. Nulls with unbroken fans are not counted in equation (1.7). By changing its unbroken status the bifurcation effectively adds or removes the null making $\Delta n = \pm 1$.

must change according to

$$\Delta X = \Delta D_{\mathrm{c}} + \frac{1}{2}\Delta D_{\phi} \quad \text{(global bifurcation)}, \tag{2.2}$$

which is equation (1.7) adapted to the case of global bifurcations. This gives us a general rule to predict the number of separators produced or destroyed by such a bifurcation, when the domain structure is known.

Following the above description we can also outline a general rule by which a global spine-fan bifurcation changes the null graph. Bifurcation $S \dashv T$ involves nulls S and T (of the same sign), where one spine of S passes through the fan of T. Let $\mathcal{S}'$ be the set of opposing null points connected directly to S by separators; let $\mathcal{T}'$ be those nulls connected to T *prior* to the bifurcation. The set $\mathcal{U}'$ of null points which will be connected to T after bifurcation $S \dashv T$ is

$$\mathcal{U}' = (\mathcal{T}' \backslash \mathcal{S}') \cup (\mathcal{S}' \backslash \mathcal{T}'). \tag{2.3}$$

The bifurcation will destroy each separator connecting T to a member of $\mathcal{T}' \cap \mathcal{S}'$, while creating new separators connecting T to each member of $\mathcal{S}' \backslash \mathcal{T}'$.

This prescription can be used to predict the topological consequences of a known global spine-fan bifurcation or to verify that such a bifurcation has occurred. We will make frequent use of this prescription in the analysis of our three evolutionary scenarios.

3. Results

(*a*) *Changing the source strength*

As the strength of the central source is increased from just above 0 up to 2 in relative units, an interesting series of topological bifurcations takes place.

In the initial state with ε very small, the flux from $P1$ is constrained by the presence of two separatrix domes (see figure 4*a*,*c*); the outer dome is the separatrix surface of $A1$, and the inner dome is the separatrix surface of $B2$. Working from equation (1.7), we have $n_{\phi}=5$, $n_{\mathrm{c}}=1$, $S=7$ and from the footprint in figure 4, $D_{\phi}=10$. There are no purely coronal domains, so $D_{\phi}=0$ and, therefore, there are $X=5$ separators. This information is summarized in the domain and null graphs, shown in figure 4*b*.

The first bifurcation to take place is the coronal local separator bifurcation. It occurs between $\varepsilon=1.21$ and 1.22 when the two separators $A3$–$B1$ and $A3$–$B2$ are pushed together until they partially join, creating two new nulls of opposite sign in the corona, which we will call $B3$ and $A5$. The new topology is shown in figure 5*a*. The original separators $A3$–$B1$ and $A3$–$B2$ now no longer exist; instead, we have new separators joining $A3$–$B3$, $A5$–$B1$, $A5$–$B2$ and $A5$–$B3$. These new null points give $\Delta n_{\mathrm{c}}=2$ in equation (2.1), which is balanced out by the change in separator count of $\Delta X=2$.

At this point, the two domes constraining the flux from $P1$ still exist—the outer dome is unchanged but the inner one is now a composite of the fan surfaces of $B2$ and $B3$. New domain and null graphs are shown in figure 5*b*. The domain graph remains unaffected by the bifurcation as it is a local bifurcation, implying

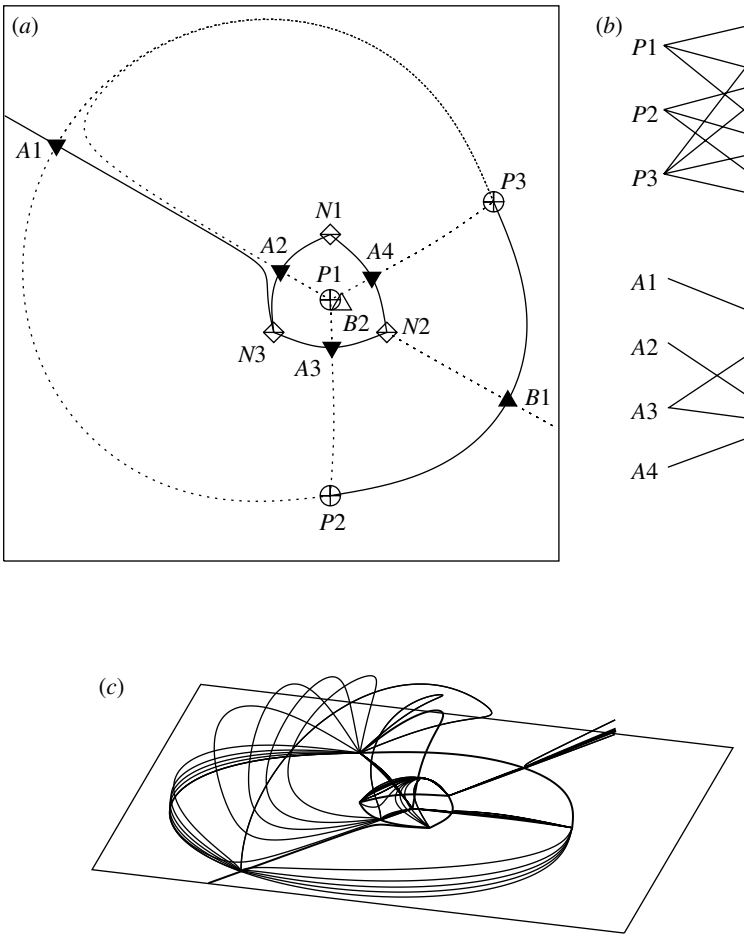

Figure 4. (*a*) The photospheric footprint when the central source strength ε is 0.7, before any bifurcations have taken place. (*b*) Domain graph (above) and null graph (below) for $\varepsilon = 0.7$. (*c*) A three-dimensional view of the corresponding topology, showing the inner and outer separatrix domes which constrain the flux from the central source.

that the structure of the flux domains staying the same, but the null graph changes significantly owing to the creation and destruction of several separators as mentioned above.

Increasing the strength of $P1$ further, the next bifurcation happens when ε passes 1.57. This is the global spine-fan bifurcation $A5 \dashv A1$ and it causes breakout, as anticipated. Figure 6*a*,*b* shows the old and new topologies, respectively, in three dimensions; the footprint is unchanged from figure 5*a*. The bifurcation itself happens when the spine of $A5$ and the fan of $A1$ approach one another, coincide and then flip past one another, creating a new flux domain linking $P1$ to $N\infty$. At the point of bifurcation, the spine forms a separator linking $A1$ to $A5$, although this state is topologically unstable. The new flux domain is purely coronal, which explains why the bifurcation cannot be detected on the photospheric footprint.

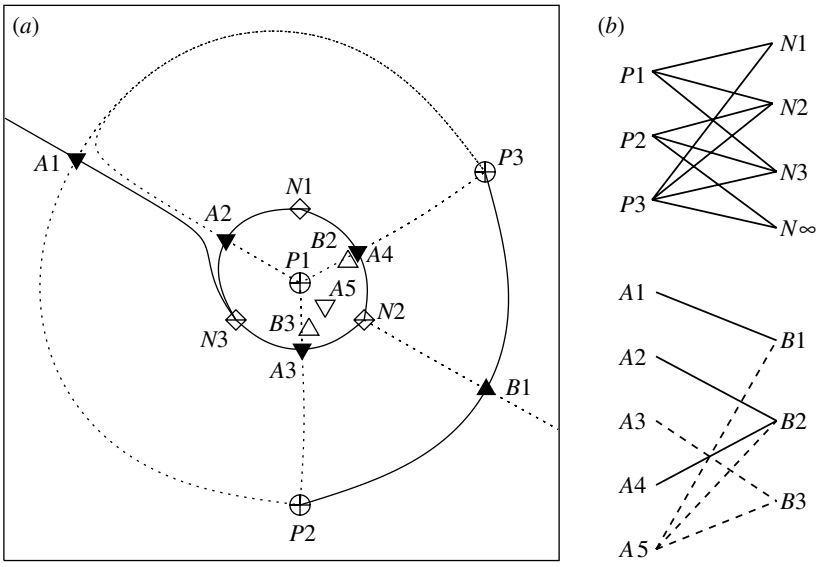

Figure 5. (*a*) The footprint at $\varepsilon = 1.3$, after the coronal local separator bifurcation. $A5$ and $B3$ are the new (coronal) nulls created in the bifurcation. (*b*) Domain graph (above) and null graph (below) after the coronal local separator bifurcation. New separators created in the bifurcation are shown as dashed lines.

To find the change in connectivity brought about by the global spine-fan bifurcation, we apply our rule from §2. Here, S is $A5$, T is $A1$, $\mathcal{S}'$ is $\{B1, B2, B3\}$ and $\mathcal{T}'$ is $\{B1\}$. Thus, after the bifurcation, $A5$ should be connected to the set of nulls $\mathcal{U}' = (\mathcal{T}' \backslash \mathcal{S}') \cup (\mathcal{S}' \backslash \mathcal{T}')$, which is $\{B2, B3\}$ in this example. This can be seen in the new domain and null graphs, given in figure 6*c*.

We also need to check that equation (2.2) is still satisfied after this global bifurcation; we have $\Delta D_c = 1$, which is balanced by the fact that on the other side $\Delta X = 1$, so the equation is indeed satisfied.

A final point to note regarding this topology is that, according to Longcope & Klapper (2002), a coronal domain such as the one produced by the global spine-fan bifurcation must be enclosed by a separator circuit. Prior to the global spine-fan bifurcation there were no separator circuits and therefore no coronal domains. The post-bifurcation null graph (figure 6*c*), with $X = 7$ separators and $n = 7$ nulls, contains $X - n + 1 = 1$ *separator circuit*. This circuit is $A1$–$B2$–$A5$–$B3$–$A1$ as can be seen in figure 6*c*; as anticipated, it engirdles the new domain $P1$–$N\infty$.

If we continue to increase the source strength, we find a local double separator bifurcation just after $\varepsilon = 1.68$. Coronal null $B2$ slides down its separator to merge with its mirror coronal partner and the photospheric null $A4$. We will continue to call the new positive photospheric null point created $B2$. The new topology can be seen in figure 7*a*.

Domain and null graphs are given in figure 7*b*. As the bifurcation is of local type, the domain graph remains unchanged. Equation (2.1) tells us that since $\Delta n_c = -1$, we should also have $\Delta X = -1$; in other words, the number of separators should decrease by 1. As predicted, the separator $A4$–$B2$ disappears during the bifurcation.

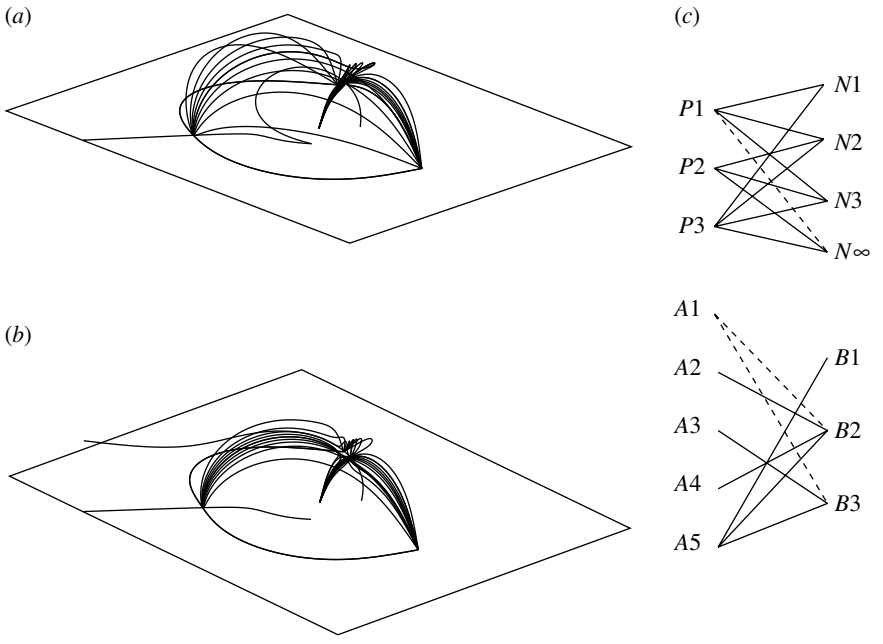

Figure 6. (*a*) A three-dimensional view of the topology just before the global spine-fan bifurcation, when the spine (thick curve) of the coronal null connects down to the photosphere. (*b*) Once the bifurcation has taken place, the spine (thick curve) reaches out to infinity. A new coronal flux domain is created, connecting the central source to infinity. This is the breakout. (*c*) Domain graph (above) and null graph (below) after the global spine-fan bifurcation. New domains and separators created in the bifurcation are shown as dashed lines.

The final bifurcation studied here occurs when ε passes 1.78; it is another local double separator bifurcation, almost a mirror of the previous one, caused by coronal null $B3$ sliding down its separator onto photospheric null $A3$. We shall call the new positive photospheric null created $B3$ to keep consistency of notation. Figure 8*a* shows the new topology.

Domain and null graphs are given in figure 8*b*. The domain graph is again unchanged as we are dealing with a local bifurcation. Identically to the last local double separator bifurcation, we have $\Delta n_{\mathrm{c}} = -1$ and $\Delta X = -1$, which satisfies equation (2.1) since the null $A3$ and the separator $A3$–$B3$ are lost in the bifurcation.

We are now well into the breakout regime, at a point where it has become obvious that increasing the source strength further will only increase the fraction of the flux of $P1$ which connects to infinity. More bifurcations may occur but they will not be able to re-enclose the flux from $P1$, so we choose to end the experiment here.

Figure 9 is a bifurcation diagram, giving a summary of where in parameter space the bifurcations occur, with the parameter in this case being the strength of the central source. It is interesting to note that, as these topologies are calculated using a potential field, if we were to start with a strong source and allow it to decrease in strength, exactly the same bifurcations would occur at the same points in parameter space.

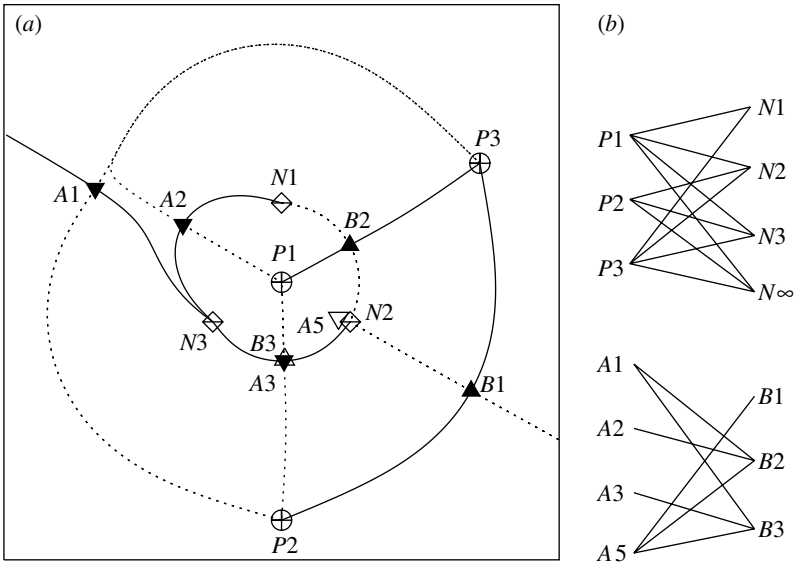

Figure 7. (*a*) The footprint at $\varepsilon = 1.7$, after the local double separator bifurcation. (*b*) Domain graph (above) and null graph (below) after the local double separator bifurcation. Note that null *A*4 has disappeared, along with its separator.

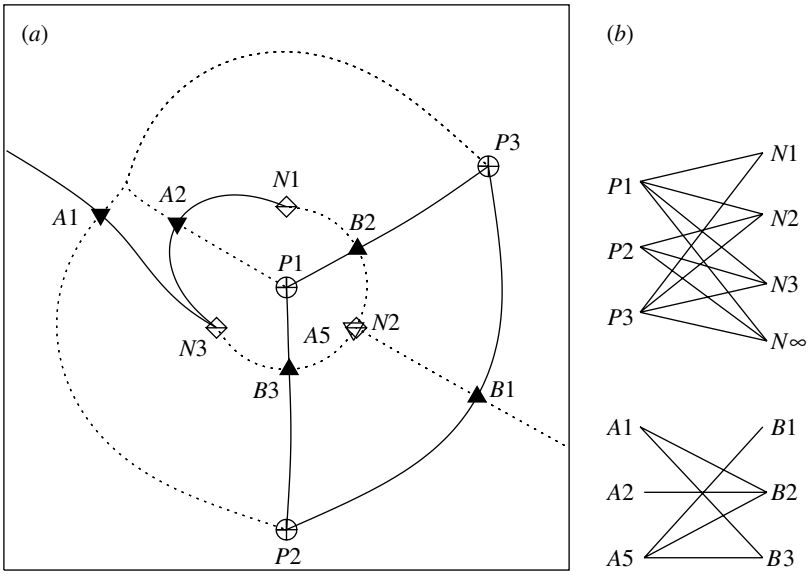

Figure 8. (*a*) The footprint at $\varepsilon = 1.8$ after the second local double separator bifurcation. *A*5 is the only remaining coronal null. (*b*) Domain graph (above) and null graph (below) after the second local double separator bifurcation. Note that null *A*3 has disappeared, along with its separator.

Thus, breakout can indeed be caused by increasing the strength of the new source. In §3*b*, we attempt to provoke breakout in a different way; by changing the position of the new source.

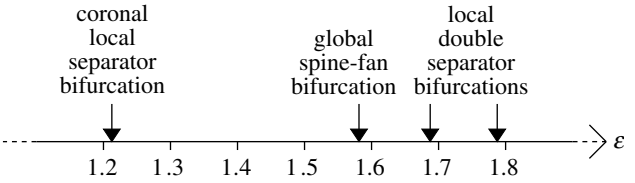

Figure 9. Bifurcation diagram as the central source strength ε changes.

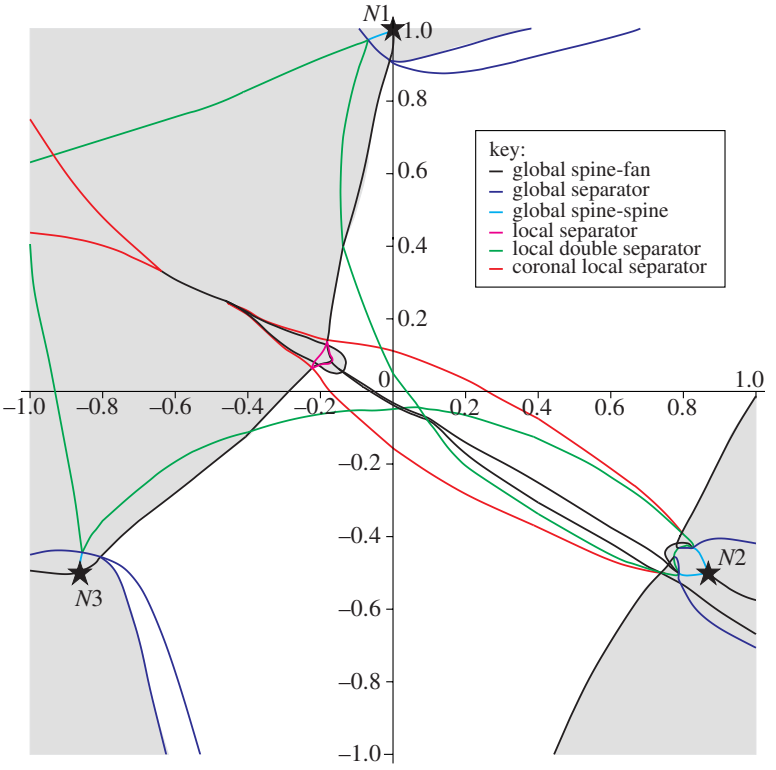

Figure 10. Bifurcation diagram created by varying each of the coordinates of the central source in the photosphere between $+1$ and -1. Shaded areas show where breakout topologies occur.

(*b*) *Changing the source position*

In this experiment there are two degrees of freedom so, unlike the previous experiment, there is no obvious order in which we can place the bifurcations that occur. As $P1$ (fixed at a relative strength of 1.5) is moved around the photosphere, breakout is observed in many distinct directions. Figure 10 is the bifurcation diagram for the square $[-1,1]\times[-1,1]$. Topologies were initially calculated and classified on a 5×5 grid within the box, then on progressively finer grids localized at the lines of bifurcation. The lowest accuracy in positioning of a bifurcation line on the diagram is ±0.01, and at some locations a much higher accuracy was required to resolve the structure, for example, the complex structure around $[-0.175,0.075]$.

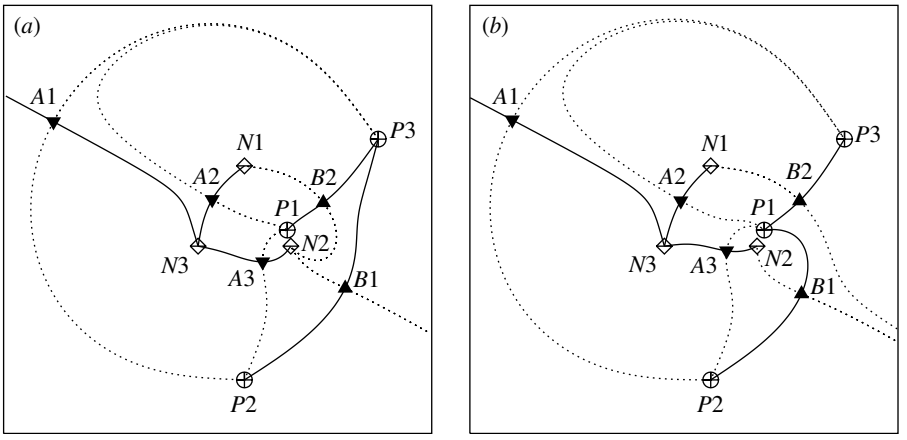

Figure 11. An example of the global spine-fan bifurcation causing breakout. The footprints are shown when the central source is at (*a*) (0.8, −0.2), before the global spine-fan bifurcation and (*b*) (1.0, −0.2), after the bifurcation. The upper spine of $B1$ changes its connection from $P3$ to $P1$, while the lower fan trace of $B2$ changes its connection from $N1$ to $N\infty$.

The diagram is almost symmetrical, owing to the fact that the five outer sources are placed in an arrangement which is close to being symmetrical. More insight can be gained through studying this almost symmetrical case than by looking at a truly symmetrical case, since some of the bifurcations are separated from each other. In the symmetrical case, for example, the two global spine-fan bifurcation lines running from the centre towards the bottom right of the bifurcation diagram would coincide.

The breakout topologies can be found in the shaded areas of the diagram. Many possible routes exist from the origin to a breakout topology. Indeed, it is believed that if the analysis were extended further out, breakout would eventually be observed in all directions as $P1$ moves far enough out from the centre to easily form a flux domain connection to $N\infty$. It is interesting to note that, although the global spine-fan bifurcation is responsible for most of the breakout behaviour, breakout can also be caused by the global separator bifurcation in some cases. Only global bifurcations can be responsible for breakout as only they can create the new flux domain required to connect $P1$–$N\infty$. Let us examine some examples of how this can happen in more detail.

Firstly, the global spine-fan bifurcation lines associated with breakout run from approximately (−0.8, −0.45) to (0, 0.9) and (0.4, −1) to (1, 0). Therefore, they account for most of the possible paths to breakout in the source configuration used. As an example, consider moving across the line of bifurcation from (0.8, −0.2) to (1, −0.2). The two topologies are shown in figure 11*a*,*b*. All the nulls here are prone, so the topology can be uniquely specified by its photospheric footprint.

The actual bifurcation is the global spine-fan bifurcation $B1 \dashv B2$, proceeding as follows. As $P1$ moves further right across the photosphere, the spine $B1$–$P3$ and the separatrix $B2$–$N2$ are pushed closer and closer together until they coincide at about $x = 0.9$ in a global spine-fan bifurcation. After the bifurcation, the spine connects $B1$–$P1$ and the separatrix connects $B2$–$N\infty$.

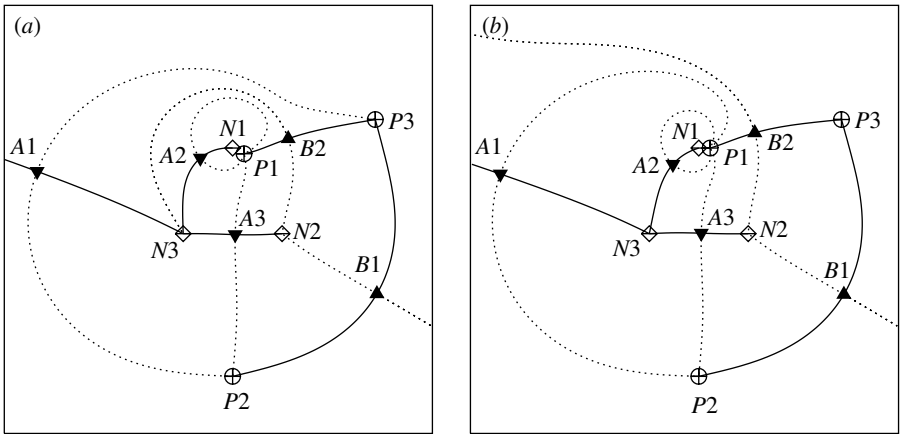

Figure 12. An example of the global separator bifurcation causing breakout. The footprints are shown when the central source is at (*a*) (0.2, 0.9), before the global separator bifurcation and (*b*) (0.2, 1.0), after the bifurcation. The upper fan trace of $A1$ changes its connection from $P3$ to $P1$, while the upper fan trace of $B2$ changes its connection from $N3$ to $N\infty$.

We apply our separator rule to find changes to the topological structure; here, with $B1$ as S and $B2$ as T, we see that $\mathcal{S}'=\{A1, A3\}$ and $\mathcal{T}'=\{A2, A3\}$ giving $\mathcal{U}'=\{A1, A2\}$. Thus, the number of separators before and after the bifurcation is constant at $X=5$. Putting this into equation (2.2) tells us that, as there are no coronal domains, the number of photospheric domains should remain unchanged. This is indeed the case; the bifurcation destroys the flux domain $P3$–$N2$ while at the same time creating a new flux domain $P1$–$N\infty$, the breakout domain.

Breakout can also be achieved via a global separator bifurcation. On the bifurcation diagram (figure 10), this can be seen in two places; an almost horizontal line of bifurcation running between the intersection with the global spine-fan bifurcation line at (0, 0.9) and (0.4, 1), and an almost vertical line running between $(-0.5, -1)$ and the intersection with the global spine-fan bifurcation line at $(-0.8, -0.6)$. Let us consider, as an example, the bifurcation involved in crossing the line between (0.2, 0.9) and (0.2, 1.0). The relevant topologies are shown in figure 12*a*,*b*.

As $P1$ moves up, the separatrices $B2$–$N3$ and $A1$–$P3$ are pushed closer together. At the point of bifurcation they coincide, and then, as $P1$ continues to move, the breakout takes place and the flux domain $P1$–$N\infty$ is created. The separatrices involved in the bifurcation change connectivity; they now join $B2$–$N\infty$ and $A1$–$P1$.

Equation (2.2) applies as we are dealing with a global bifurcation. This time we have $\Delta X=1$ as a new separator, $A1$–$B2$, is created. The equation holds because $\Delta D_{\mathrm{c}}=1$ as flux domain $P3$–$N3$ is pushed up into the corona by the bifurcation, changing its classification from photospheric to coronal. $\Delta D_{\phi}=0$ because the creation of the (photospheric) breakout domain $P1$–$N\infty$ balances the loss of the domain $P3$–$N3$ to the corona.

Thus we have seen that breakout behaviour can be indeed provoked by moving a newly emerging flux source across the photosphere, and that two distinct global bifurcations can be responsible for this effect. In §3*c* we work with

force-free instead of potential fields, to test whether breakout can be caused by changing the parameter α of the force-free field.

(c) *Changing the force-free parameter* α

A sequence of non-potential fields will probably exhibit similar types of topological change to the potential fields considered so far, provided they are not too far from potential. To demonstrate this, we construct linear force-free fields for the same distribution of photospheric sources. Linear force-free fields are one step closer to reality than potential ones, allowing us to add helicity to the field and, if the same types of changes occur in both, giving us a higher degree of confidence in the qualitative predictions of our model. Of course, a nonlinear force-free field would be a better approximation still but the complexity of such simulations leads us to consider the linear case for now. A disadvantage of linear force-free fields is that they are energetically unbounded but they can still give us a great deal of information about local field topologies.

The linear force-free field for a given α is computed by summing up the contributions of all sources; the contribution of each source is given by a Green's function (Chiu & Hilton 1977). In the vicinity of its source the Green's function is radial and diverges as r^{-2}, exactly the same as for the potential field. However, at distances beyond $\pi/2|\alpha|$ the radial field oscillates, ultimately only falling off as r^{-1}. Therefore, linear force-free fields cannot be used to model fields outside a distance of $\pi/2|\alpha|$ from each source. We restrict our consideration to this region and refer to the field lines exiting it as extending to 'infinity'.

Sequences of equilibria in which $|\alpha|$ increases from zero show some of the same bifurcations explored in the previous sections, including, in some cases, breakout. The particular distribution with $\varepsilon = 1.5$ and source $P1$ located at $(-0.05, 0.05)$ is a useful illustration. The bifurcation diagram, figure 10, shows that the potential field has the same topology as the case with $P1$ at the origin, whose footprint is shown in figure 2. Three global spine-fan bifurcations occur as α is made increasingly negative, beginning at zero. The first, $A1 \dashv A2$, occurs at $\alpha = -0.011$. Since $\mathcal{S}' = \{B1\}$ and $\mathcal{T}' = \{B2\}$ we find that $\mathcal{U}' = \{B1,\ B2\}$, implying the creation of the new separator $A2$–$B1$. This adds the photospheric domain $P2$–$N1$, and converts the photospheric domain $P3$–$N3$ into a coronal domain engirdled by the newly created separator circuit $A2$–$B1$–$A5$–$B2$–$A2$.

The second bifurcation, $A5 \dashv A2$, occurs at $\alpha = -0.028$. This destroys separators $A2$–$B1$ and $A2$–$B2$ and creates separator $A2$–$B3$ ($\Delta X = -1$), destroying the separator circuit and with it the coronal domain $P3$–$N3$ ($\Delta D_c = -1$). The resulting topology is shown by the footprint and graphs in figure 13*a*,*b*, for $\alpha = -0.1$. Source $P1$ now connects to $N1$, $N2$ and $N3$ in domains lying underneath a dome formed by the fan surfaces of $B2$ and $B3$, which join along the spines of coronal null $A5$.

The third global spine-fan bifurcation, $A5 \dashv A1$, occurs at $\alpha = -0.197$, taking the spine of $A5$ to 'infinity' (i.e. beyond $r \simeq 7.5$). The bifurcation destroys separator $A1$–$B1$ and creates separators $A2$–$B1$ and $A3$–$B1$ ($\Delta X = 1$). This forms a separator circuit $A2$–$B2$–$A3$–$B3$–$A2$ engirdling a new coronal domain, $P1$–$N\infty$, which is the breakout domain. Figure 14 shows field lines, for $\alpha = -0.21$, from the breakout domain and two of the domains which had been under the dome prior to breakout. Note that the sequence of three global

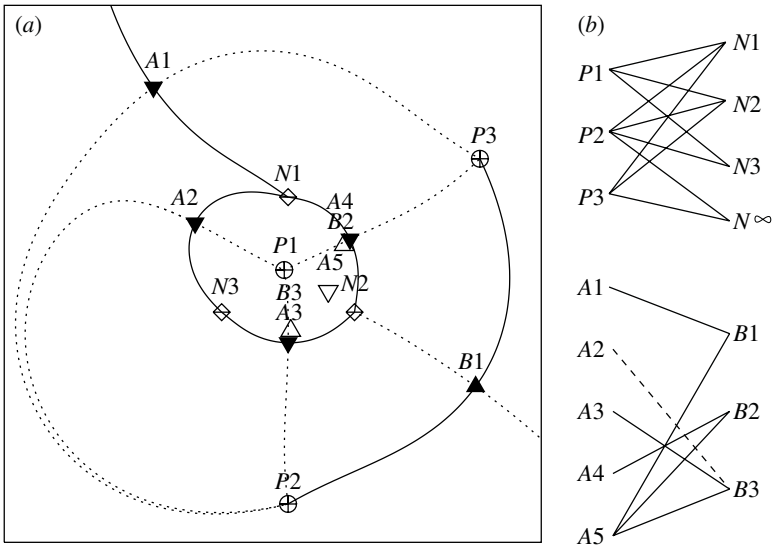

Figure 13. (*a*) The footprint of the force-free field $\alpha = -0.1$ with $\varepsilon = 1.5$, and source $P1$ at $(-0.05, 0.05)$. (*b*) Domain and null graphs for this topology.

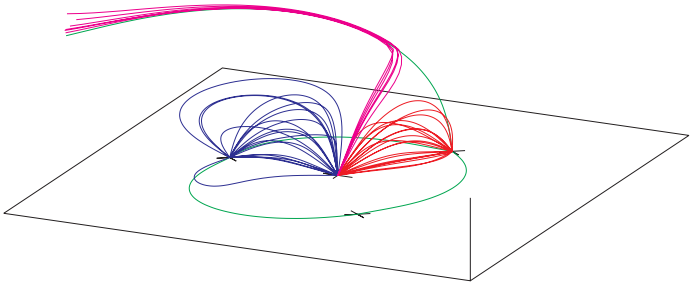

Figure 14. Field lines from a force-free field with the same source configuration as figure 13 but $\alpha = 0.21$—beyond the breakout bifurcation. Green lines in the photosphere are the spines of the photospheric nulls $A1$, $A2$ and $A3$. The red and blue field lines which close down to the photosphere are from domains $P1$–$N2$ and $P1$–$N3$. The magenta field lines which extend out of the diagram to the top left are from $P1$–$N\infty$, the flux domain created by breakout.

spine-fan bifurcations, $A1 \dashv A2$, $A5 \dashv A2$ and $A5 \dashv A1$, in the force-free evolution has accomplished the same topological change as the single bifurcation $A5 \dashv A1$ which occurred in the potential evolution at $\varepsilon = 1.57$.

Hence, we have seen that varying the parameter α of a force-free field can lead to breakout behaviour. The manner in which the breakout proceeds is very similar to the previous potential field calculations, suggesting that a potential field gives a good qualitative picture of the topological behaviour of our sunspot.

4. Discussion

Antiochos *et al.*'s (1999) conception of the magnetic breakout model is far more complex than can be expressed with a potential field, accounting as it does for the

Figure 15. Two TRACE images of AR9574, showing the formation of a new magnetic connection between two previously separate regions of flux (from Longcope *et al.* submitted).

energy storage necessary in the run-up to a flare, since potential fields are incapable of storing excess energy. However, we have shown that our simple potential field model of a delta sunspot can display topological breakout behaviour in several distinct ways—by moving the flux sources or by altering the source strengths. A slightly more complicated, linear force-free field model can also be made to 'break out' by altering the parameter α.

We have demonstrated that at least two different global topological bifurcations can provide a mechanism for breakout: the global spine-fan bifurcation and the global separator bifurcation. In fact, it seems that breakout behaviour is ubiquitous in our delta sunspot model; whichever parameter is varied, the system can eventually make its way towards a breakout configuration.

We have also derived rules governing the number of separators created or destroyed in both local and global bifurcations (equations (2.1) and (2.2)), as well as a rule predicting the exact changes to the topological skeleton brought about by a global spine-fan bifurcation (equation (2.3)). Topological rules such as these are very useful in checking that calculated topologies are indeed correct and self-consistent.

It is interesting to note that these results could also be applied to active region structures, explaining how distant magnetic connections can appear suddenly where before there were none. Figure 15 shows an example from TRACE of loop-like structures forming to connect previously separated regions of flux in AR9574 (Longcope *et al.* submitted). Our results suggest that this new flux domain forms as a result of a global bifurcation; detailed modelling would be required to determine its exact nature.

We hope that this work will pave the way for a deeper topological understanding of the magnetic breakout model.

We are grateful to the UK Particle Physics and Astronomy Research Council for funding and to the three anonymous referees for their helpful and insightful comments.

References

Antiochos, S. K. 1998 The magnetic topology of solar eruptions. *Astrophys. J.* **502**, L181–L184.

Antiochos, S. K., DeVore, C. R. & Klimchuk, J. A. 1999 A model for solar coronal mass ejections. *Astrophys. J.* **510**, 485–493.

Beveridge, C. 2003 Magnetic topology of the solar corona. Ph.D. thesis, University of St. Andrews.

Beveridge, C., Brown, D. S. & Priest, E. R. 2005 Magnetic topologies in the solar corona due to four discrete photospheric flux regions. *Geophys. Astrophys. Fluid Dyn.* **98**, 429–445.

Brown, D. S. & Priest, E. R. 1999 Topological bifurcations in three-dimensional magnetic fields. *Proc R. Soc. A* **455**, 3931–3951. (doi:10.1098/rspa.1999.0484.)

Brown, D. S. & Priest, E. R. 2000 Topological differences and similarities between force-free and potential models of coronal magnetic fields. *Solar Phys.* **194**, 197–204.

Chiu, Y. T. & Hilton, H. H. 1977 Exact Green's function method of solar force-free magnetic-field computations with constant alpha. I. Theory and basic test cases. *Astrophys. J.* **212**, 873–885.

Démoulin, P., Priest, E. R. & Lonie, D. P. 1996 Three-dimensional magnetic reconnection without null points. 2. Application to twisted flux tubes. *J. Geophys. Res.* **101**, 7631–7646.

Galsgaard, K. & Nordlund, Å. 1997 Heating and activity of the solar corona. 3. Dynamics of a low beta plasma with three-dimensional null points. *J. Geophys. Res.* **102**, 231–248.

Gary, G. A., Moore, R. L., Hagyard, M. J. & Haisch, B. M. 1987 Nonpotential features observed in the magnetic field of an active region. *Astrophys. J.* **314**, 782–794.

Gerrard, C. L. & Hood, A. W. 2003 Kink unstable coronal loops: current sheets, current saturation and magnetic reconnection. *Solar Phys.* **214**, 151–169.

Greene, J. M. 1988 Geometrical properties of three-dimensional reconnecting magnetic fields with nulls. *J. Geophys. Res.* **93**, 8583–8590.

Hornig, G. & Schindler, K. 1996 Magnetic topology and the problem of its invariant definition. *Phys. Plasmas* **3**, 781–792.

Inverarity, G. & Priest, E. R. 1999 Magnetic null points due to multiple sources of solar photospheric flux. *Solar Phys.* **186**, 99–121.

Klimchuk, J. A. & Sturrock, P. A. 1989 Force-free magnetic fields—is there a 'loss of equilibrium'? *Astrophys. J.* **345**, 1034–1041.

Klimchuk, J. A. & Sturrock, P. A. 1992 Three-dimensional force-free magnetic fields and flare energy buildup. *Astrophys. J.* **385**, 344–353.

Lau, Y. T. & Finn, J. M. 1990 Three-dimensional kinematic reconnection in the presence of field nulls and closed field lines. *Astrophys. J.* **350**, 672–691.

Longcope, D. W. 1996 Topology and current ribbons: a model for current, reconnection and flaring in a complex, evolving corona. *Solar Phys.* **169**, 91–121.

Longcope, D. W. 2001 Separator current sheets: generic features in minimum-energy magnetic fields subject to flux constraints. *Phys. Plasmas* **8**, 5277–5290.

Longcope, D. W. & Klapper, I. 2002 A general theory of connectivity and current sheets in coronal magnetic fields anchored to discrete sources. *Astrophys. J.* **579**, 468–481.

Longcope, D. W. & Magara, T. 2004 A comparison of the minimum current corona to a magnetohydrodynamic simulation of quasi-static coronal evolution. *Astrophys. J.* **608**, 1106–1123.

Longcope, D. W., McKenzie, D. E., Cirtain, J. & Scott, J. Submitted. Observations of separator reconnection to an emerging active region.

McLaughlin, J. A. & Hood, A. W. 2004 MHD wave propagation in the neighbourhood of a two-dimensional null point. *Astron. Astrophys.* **420**, 1129–1140.

Molodenskii, M. M. & Syrovatskii, S. I. 1977 Magnetic fields of active regions and their zero points. *Sov. Astron.* **21**, 734–741.

Moore, R. L., Sterling, A. C., Hudson, H. S. & Lemen, J. R. 2001 Onset of the magnetic explosion in solar flares and coronal mass ejections. *Astrophys. J.* **552**, 833–848.

Parnell, C. E., Smith, J. M., Neukirch, T. & Priest, E. R. 1996 The structure of three-dimensional magnetic neutral points. *Phys. Plasmas* **3**, 759–770.

Priest, E. R. & Démoulin, P. 1995 Three-dimensional magnetic reconnection without null points. 1. Basic theory of magnetic flipping. *J. Geophys. Res.* **100**, 23 443–23 464.

Priest, E. R. & Forbes, T. G. 1990 Magnetic field evolution during prominence eruptions and two-ribbon flares. *Solar Phys.* **126**, 319–350.

Priest, E. R. & Titov, V. S. 1996 Magnetic reconnection at three-dimensional null points. *Phil. Trans. R. Soc. A* **354**, 2951–2992.

Priest, E. R., Bungey, T. N. & Titov, V. S. 1997 The 3D topology interaction of complex magnetic flux systems. *Geophys. Astrophys. Fluid Dyn.* **84**, 127–163.

Tanaka, K. 1991 Studies on a very flare-active delta group—peculiar delta SPOT evolution and inferred subsurface magnetic rope structure. *Solar Phys.* **136**, 133–149.

Titov, V. S., Hornig, G. & Démoulin, P. 2002 Theory of magnetic connectivity in the solar corona. *J. Geophys. Res.* **107**, SSH3-1.

Török, H., Kliem, B. & Titov, V. S. 2004 Ideal kink instability of a magnetic loop equilibrium. *Astron Astrophys.* **413**, L27–L30.

Zhang, H. 1995 Magnetic shear of a large delta sunspot group (NOAA 6659) in June 1991. *Astron. Astrophys.* **297**, 869–880.

Zhang, M. & Low, B. C. 2001 Magnetic flux emergence into the solar corona. I. Its role for the reversal of global coronal magnetic fields. *Astrophys. J.* **561**, 406–419.

Zhang, M. & Low, B. C. 2003 Magnetic flux emergence into the solar corona. III. The role of magnetic helicity conservation. *Astrophys. J.* **584**, 479–496.